Turbulent Fluxes of Liquid Water and Buoyancy in Partly Cloudy Layers

DAVID A. RANDALL

Laboratory for Atmospheres, NASA/Goddard Space Flight Center, Greenbelt, MD 20771

(Manuscript received 7 April 1986, in final form 29 September 1986)

ABSTRACT

A simple convective mass flux model is used to derive expressions for the fluxes of liquid water and buoyancy in partly cloudy turbulent layers. The results differ radically from those suggested in some previous studies. Physical interpretation is given, and examples are presented. Implications for the dynamics of partly cloudy boundary layers are discussed, and the aftermath of cloud-top entrainment instability is analyzed.

1. Introduction

In formulating boundary layer models, it is often necessary to determine the rate at which turbulence kinetic energy is generated by buoyant convection, which is proportional to the turbulent flux of virtual dry static energy (hereafter, the "buoyancy flux"). In general, the buoyancy flux can be written as (Randall, 1980a)

$$F_{sv} = F_h - (1-\delta\epsilon)LF_r + [1-(1+\delta)\epsilon]LF_l. \quad (1.1)$$

Here F_h, F_r and F_l are the turbulent fluxes of moist static energy, total moisture (liquid plus vapor), and liquid water, respectively; $\delta \approx 0.608$ is a function of the ratio of the molecular weight of water vapor to that of dry air; $\epsilon \equiv c_pT/L$; c_p is the specific heat of air at constant pressure; T is temperature; and L is the latent heat of condensation. The moist static energy, h, and total water mixing ratio, r, are convenient variables to use when clouds are considered, because they are conserved under both moist adiabatic and dry adiabatic processes. According to (1.1), for given moist static energy and total water fluxes, an upward liquid water flux promotes an upward buoyancy flux. In the absence of clouds, the liquid water flux vanishes, so that the buoyancy flux can be expressed simply as a linear combination of the moist static energy and total water fluxes:

$$F_{sv} = (F_{sv})_{CLR} \equiv F_h - (1-\delta\epsilon)LF_r. \quad (1.2)$$

Lilly (1968) pointed out that an analogous simplification can be made for a uniformly saturated layer. There temperature fluctuations are proportional to vapor fluctuations, and it follows that the liquid water flux satisfies

$$LF_l = (LF_l)_{CLD} \equiv LF_r - \left(\frac{\gamma}{1+\gamma}\right)F_h, \quad (1.3)$$

where

$$\gamma \equiv \frac{L}{c_p}\left(\frac{\partial q^*}{\partial T}\right)_p. \quad (1.4)$$

Here q^* is the saturation mixing ratio, and p is pressure. Using (1.3) in (1.1), we find that

$$F_{sv} = (F_{sv})_{CLD} \equiv \left[\frac{1+(1+\delta)\gamma\epsilon}{1+\gamma}\right]F_h - \epsilon LF_r. \quad (1.5)$$

This result, due to Lilly, demonstrates that, for uniformly saturated air, the buoyancy flux can again be expressed as a linear combination of the moist static energy and total water fluxes.

In reality, both completely clear skies and uniformly cloudy skies are rare occurrences; partial cloudiness is the rule, and a method is needed to determine the turbulent fluxes of liquid water and buoyancy in partly cloudy air. In this paper we consider only "intrinsic" fractional cloudiness, as defined by Randall (1985). A partial cloudiness parameterization intended for use in large-eddy models, with grid volumes on the order of $(100\ \text{m})^3$, was suggested by Sommeria and Deardorff (1977) and Mellor (1977). They showed that the fractional cloudiness can be determined if the temperature and total mixing ratio in partly cloudy air have a Gaussian joint distribution whose means, variances, and covariance are known. Sommeria and Deardorff suggested that the buoyancy flux in such a layer satisfies

$$F_{sv} = \sigma(F_{sv})_{CLD} + (1-\sigma)(F_{sv})_{CLR}, \quad (1.6)$$

where σ is the fractional cloudiness, and $(F_{sv})_{CLD}$ and $(F_{sv})_{CLR}$ are given by (1.5) and (1.2), respectively. The corresponding liquid water flux satisfies

$$LF_l = \sigma(LF_l)_{CLD}, \quad (1.7)$$

where $(LF_l)_{CLD}$ is given by (1.3). To verify (1.6), Sommeria and Deardorff generated joint normal distributions of h, r, and the vertical velocity, and by computing covariances examined the relationships between the fluxes of buoyancy, moist static energy, and total moisture. They found that (1.6) was well satisfied.

Oliver et al. (1978), Yamada and Mellor (1979), and

Banta and Cotton (1980) used methods similar to those suggested by Sommeria and Deardorff, but applied them in higher-order closure models, whose grid volumes represent mesoscale horizontal areas, large enough to contain many "large" turbulent eddies, and comparable to the grid size of a general circulation model. Bougeault (1981, 1982) questioned whether the joint distributions of the thermodynamic variables are normal on such scales. He suggested that in a field of scattered cumuli the distributions of the thermodynamical fields and vertical velocity have large skewness, since the narrow, cloudy updrafts are characterized by relatively large departures from the mean, while the broad clear descending environment has properties relatively close to the mean. Bougeault presented evidence for this idea from high-resolution three-dimensional numerical simulations, and he remarked that in some cases the simulated shallow cloud fields showed bimodal distributions of the thermodynamic variables and the vertical velocity.

In this paper a "convective mass flux" model, similar to that first used in a theory of deep and shallow cumulus convection by Arakawa (1969), and later applied to shallow convection by Betts (1973), is used to derive expressions for the fluxes of liquid water and buoyancy in partly cloudy turbulent layers. The results are strongly at odds with (1.6) and (1.7), and the reasons for this are examined. Implications for the dynamics of partly cloudy boundary layers are discussed.

2. Mass flux model

Consider a single family of convective circulations, consisting of ascending and descending branches covering fractional areas σ and $(1-\sigma)$, respectively. For any scalar Ψ, we can write

$$\bar{\Psi} = \sigma\Psi_u + (1-\sigma)\Psi_d. \tag{2.1}$$

Here the overbar denotes an areal mean, and subscripts u and d denote the upward and downward branches respectively. Let

$$\omega \equiv -\rho g w, \tag{2.2}$$

where ρ is density, g is the acceleration of gravity, and w is vertical velocity (positive upward). Then the upward flux of Ψ due to the convective circulations satisfies

$$\begin{aligned} -gF_\Psi &= \sigma(\omega_u-\bar{\omega})(\Psi_u-\bar{\Psi}) + (1-\sigma)(\omega_d-\bar{\omega})(\Psi_d-\bar{\Psi}) \\ &= \omega_*(\Psi_u-\Psi_d), \end{aligned} \tag{2.3}$$

where

$$\omega_* \equiv \sigma(1-\sigma)(\omega_u-\omega_d) \tag{2.4}$$

is the "convective mass flux." Note that (2.3) applies for any value of σ, with or without mean vertical motion, and that $\omega_* \leq 0$. A fundamental assumption of this paper is that the fluctuations and fluxes of moist static energy, total mixing ratio, and liquid water in a shallow partly cloudy convective layer are well described by (2.1)–(2.4). Evidence for this is reviewed in the Appendix.

The liquid water mixing ratio of the updraft is

$$\begin{aligned} l_u &= \max\{r_u - q_u^*, 0\} \\ &= \max\{(r_u-\bar{r}) + (\bar{r}-\tilde{q}_*) + (\tilde{q}_* - q_{*u}), 0\}, \end{aligned} \tag{2.5}$$

where $\tilde{q}_*$ is the saturation mixing ratio at temperature $\tilde{T}$. We do not specify $\tilde{T}$ for now. From the Clausius–Clapeyron equation, we can show that

$$\begin{aligned} L(\tilde{q}_* - q_{*u}) &= \left(\frac{\gamma}{1+\gamma}\right)(\tilde{h}_* - h_u^*) \\ &= \left(\frac{\gamma}{1+\gamma}\right)[(\tilde{h}_*-\bar{h}) - (h_u-\bar{h})]. \end{aligned} \tag{2.6}$$

Here h^* is the saturation moist static energy, and we have used $h_u = h_u^*$, which is correct only when the updraft is saturated. Using (2.6) in (2.5), we obtain

$$Ll_u = \max\left\{L\tilde{l} + \left[L(r_u-\bar{r}) - \left(\frac{\gamma}{1+\gamma}\right)(h_u-\bar{h})\right], 0\right\}, \tag{2.7}$$

where

$$L\tilde{l} \equiv L(\bar{r}-\tilde{q}_*) - \left(\frac{\gamma}{1+\gamma}\right)(\bar{h}-\tilde{h}_*). \tag{2.8}$$

At this point, our expression for Ll_u involves differences between the properties of the updrafts and those of the mean state. We now use (2.1) to rewrite these in terms of differences between the properties of the updrafts and downdrafts; then (2.7) becomes

$$\begin{aligned} Ll_u = \max\Bigg\{&L\tilde{l} + (1-\sigma) \\ &\times\left[L(r_u-r_d) - \left(\frac{\gamma}{1+\gamma}\right)(h_u-h_d)\right], 0\Bigg\}. \end{aligned} \tag{2.9}$$

In a similar way, we can show that the liquid water mixing ratio of the downdraft is

$$Ll_d = \max\left\{L\tilde{l} - \sigma\left[L(r_u-r_d) - \left(\frac{\gamma}{1+\gamma}\right)(h_u-h_d)\right], 0\right\}. \tag{2.10}$$

In order to choose $\tilde{T}$, we consider the case in which both the updraft and downdraft are saturated. Then from (2.1), (2.9), and (2.10) we get

$$L\bar{l} = \sigma Ll_u + (1-\sigma)Ll_d = L\tilde{l}. \tag{2.11}$$

This will make sense if we chose $\tilde{T} = \bar{T}$, so that $\tilde{q}_* = \bar{q}_* = \bar{q}$, and $\tilde{h}_* = \bar{h}_* = \bar{h}$; then from (2.11) and the definition of $\tilde{l}$ we get $\bar{l} = \bar{r} - \bar{q}$. If the updraft and downdraft are both saturated, $\tilde{l}$ is positive and equal to $\bar{l}$. If only the updraft is saturated, it is possible for $\tilde{l}$ to be negative. When $\tilde{l}$ is negative, $-\tilde{l}$ can be interpreted as the amount of liquid that would have to be isobar-

ically evaporated into the mean state to bring it to saturation. In general, $\tilde{l}$ is a measure of the relative humidity of the mean state.

Now define

$$LF_{lu} \equiv -\frac{\omega_*}{g} Ll_u \geq 0, \tag{2.12}$$

$$LF_{ld} \equiv \frac{\omega_*}{g} Ll_d \leq 0, \tag{2.13}$$

so that, from (2.3), the total liquid water flux can be expressed as

$$LF_l = -\frac{\omega_*}{g} L(l_u - l_d) = LF_{lu} + LF_{ld}. \tag{2.14}$$

Using (2.9), (2.10), (2.12), (2.13) and (1.3), we find that

$$LF_{lu} = \max\left\{(1-\sigma)(LF_l)_{\mathrm{CLD}} - \frac{\omega_*}{g} L\tilde{l}, 0\right\}, \tag{2.15}$$

$$LF_{ld} = \min\left\{\sigma(LF_l)_{\mathrm{CLD}} + \frac{\omega_*}{g} L\tilde{l}, 0\right\}. \tag{2.16}$$

If both updraft and downdraft are saturated, we can combine (2.14–16) to recover (1.3), which is Lilly's (1968) result for uniformly saturated air.

We are now ready to give expressions for the fluxes of liquid water and buoyancy in partly cloudy layers. Consider a case in which the updraft contains liquid ($l_u > 0$) but the downdraft does not ($l_d = 0$). Then the liquid water flux can be obtained directly from (2.15):

$$LF_l = (1-\sigma)(LF_l)_{\mathrm{CLD}} - \frac{\omega_*}{g} L\tilde{l}. \tag{2.17}$$

By combining (1.1), (1.2) and (1.5) with (2.17) we can obtain an expression for the buoyancy flux:

$$F_{sv} = (1-\sigma)(F_{sv})_{\mathrm{CLD}} + \sigma(F_{sv})_{\mathrm{CLR}} - \frac{\omega_*}{g}[1-(1+\delta)\epsilon]L\tilde{l}. \tag{2.18}$$

3. Interpretations and illustrations

The main results of section 2 are expressed by (2.17) and (2.18), which have been derived by straightforward application of a familiar convection model. These results are paradoxical and counterintuitive, and differ radically from (1.7) and (1.6), which are the corresponding very plausible suggestions of Sommeria and Deardorff (1977). According to (2.17), the liquid water flux actually increases as the fractional cloudiness decreases! Similarly, in the expression for the buoyancy flux in partly cloudy air given by (2.18), $(F_{sv})_{\mathrm{CLD}}$ is weighted by the fraction of clear air, and $(F_{sv})_{\mathrm{CLR}}$ is weighted by the fraction of cloudy air! Also, LF_l and F_{sv} are not just weighted sums of F_h and LF_r; they also depend on the product of the convective mass flux and $\tilde{l}$. In the limit as $\sigma \to 0$, and if $\tilde{l} = 0$, LF_l and F_{sv} approach the values that they would take in a fully saturated layer with the same moist static energy and total water fluxes.

An interpretation is as follows. Inspection of (2.1) shows that as σ decreases, for a given difference between the updraft and downdraft properties, the updraft's properties differ increasingly from those of the mean, while the downdraft's properties become increasingly close to those of the mean. The liquid water content of the cloudy updrafts increases as σ decreases, but that of the clear downdrafts remains constant (at zero). It is this *asymmetry between the moist updrafts and the dry downdrafts* that causes LF_l and F_{sv} to increase as σ decreases.

The present results bring to mind to those of Bjerknes (1938), who showed that the buoyancy of cloudy updrafts in a clear descending environment is maximized in the limit as the fractional area covered by the updrafts approaches zero. However, Bjerknes' study involved consideration of the differing lapse rates in the cloud and environment, while lapse rates do not enter into the present analysis.

Our results can be applied directly to interpret the "two-cylinder" cloud model developed by Asai and Kasahara (1967). They showed that the vertical heat transport by their model clouds is largest when the fractional area covered by rising motion is small. The present analysis is consistent with their results. They suggested that the clouds organize themselves so as to maximize the upward heat transport, and that this accounts for the observed tendency for moist convective updrafts to occupy a small fraction of a synoptic circulation within which they occur. A full discussion of this point requires a method to determine ω_* and σ; that is outside the scope of the present paper.

For $\tilde{l} \approx 0$, it appears that the buoyancy flux can attain its largest possible value, $(F_{sv})_{\mathrm{CLD}}$, *either* in a fully overcast layer with $\sigma \simeq 0.5$, *or* in a partly cloudy layer with $\sigma \ll 1$. This is an intriguing idea, because it suggests that stratocumulus convection and shallow cumulus convection, which are superficially very different, are energetically similar. Such a similarity might help to explain the abrupt transitions between stratocumulus and shallow cumulus convection that are sometimes observed. Caution is needed, however, because this line of argument is based on the premise that $(F_{sv})_{\mathrm{CLD}}$ is fixed. In reality, the turbulent fluxes in a cloudy layer are driven in part by the interaction between the clouds and radiation. Decreased fractional cloudiness is likely to be accompanied by weaker area-averaged cloud-top radiative cooling, which will tend to favor weaker fluxes and in particular smaller values of F_h. For this reason, $(F_{sv})_{\mathrm{CLD}}$ itself will tend to be smaller in a partly cloudy layer than in a fully overcast layer with the same mean thermodynamic structure. Radiation effects thus complicate the interpretation of our results. This becomes more apparent in the next section.

To illustrate how the liquid water and buoyancy fluxes vary with σ and ω_*, consider a "typical" stratocumulus or shallow cumulus case, with the conditions given in Table 1. These conditions correspond to a mean temperature of 283.8 K and a mean relative humidity of 98.7%, with $\tilde{l} = -0.044$ g kg^{-1}, $(F_{sv})_{CLR} = 25.5$ W m^{-2}, $(F_{sv})_{CLD} = 42.9$ W m^{-2}, and $(LF_l)_{CLD} = 21.3$ W m^{-2}. Using the parameters of Table 1 as input, and with selected values of σ and ω_*, we can apply the results of section 2 to evaluate the liquid water and buoyancy fluxes, as well as the properties of the updrafts and downdrafts. We consider $0.01 \leq \sigma \leq 0.99$, and 10 mb hr$^{-1} \leq -\omega_* \leq 100$ mb h^{-1}.

Figure 1a shows how l_u varies with σ and ω_*. For large $|\omega_*|$, only small fluctuations of h and r are needed to account for F_h and F_r, and the updraft is unsaturated for all values of σ. As $|\omega_*|$ decreases, $l_u > 0$ occurs first for small values of σ, which give updraft properties quite different from the mean. The largest values of l_u are obtained for small $|\omega_*|$ and small σ. However, Fig. 1b shows that the *mean* liquid water is maximized for small $|\omega_*|$ and intermediate values of σ, since narrow updrafts contribute little to the area average. The variation of LF_l [which for this case is the same as $(LF_l)_u$] with σ and ω_* is shown in Fig. 1c. Again, the largest values occur for small $|\omega_*|$ and small σ. The same is true for F_{sv}, as shown in Fig. 1d.

To illustrate some implications of the convective mass flux model for the vertical structure of cloudy boundary layers, consider a cloud-topped well-mixed layer with vertically uniform values of F_h and F_r. The parameters of Table 1 are used again, except that p is allowed to vary from 1020 mb at the earth's surface to 940 mb at the top of the mixed layer, and z is determined hydrostatically using $z = 0$ at the earth's surface. We consider $\sigma = 0.5$. Attention is focused on the levels near the mean cloud base, where the mean-state relative humidity is near 100% and $\tilde{l}$ is near zero. We can use $\tilde{l}$ as a vertical coordinate; it increases upward from $\tilde{l} = -0.1$ g kg^{-1} to $\tilde{l} = 0.1$ g kg^{-1} through a layer approximately 110 m deep, centered at $z \approx 520$ m. Figure 2 shows the variation with $\tilde{l}$ of l_u, l_d, $\bar{l}$, $(LF_l)_u$, $(LF_l)_d$, $-(\omega_*/g)L\tilde{l}$, LF_l and F_{sv}. The cloud base for the updrafts is about 55 m lower than that for the downdrafts. Within the partly cloudy layer between the two cloud base levels, $\bar{l}$ increases upward from zero to $\tilde{l}$, LF_l increases upward from zero to $(LF_l)_{CLD}$, and F_{sv} increases upward from $(F_{sv})_{CLR}$ to $(F_{sv})_{CLD}$. All three transitions are gradual. In contrast, conventional cloud-topped mixed-layer models of the type introduced by Lilly (1968) predict that LF_l and F_{sv} are discontinuous at the "mean" cloud base, where $\bar{l} = 0$.

TABLE 1. Parameters in the examples of section 3.

$p = 960$ mb
$z = 500$ m
$\bar{h}/c_p = 309.5$ K
$\bar{r} = 8.3$ g kg^{-1}
$F_h = 100$ W m^{-2}
$LF_r = 80$ W m^{-2}

In the upper region of the partly cloudy layer, where $\tilde{l} > 0$, an increase in $|\omega_*|$ with all other parameters fixed will cause both the updraft and downdraft properties to approach the mean and ultimately to reach saturation. In other words, this region can be *either* partly cloudy *or* overcast, depending on the value of ω_* (and also depending on F_h, F_r, and σ). Similarly, the lower region where $\tilde{l} < 0$ can be *either* partly cloudy *or* clear.

4. The aftermath of cloud-top entrainment instability

Cloud-top entrainment instability is a hypothetical process that has been proposed as a mechanism for the destruction of a layer cloud (Lilly, 1968; Randall, 1976a; Deardorff, 1980a) and its replacement by a field of shallow cumuli. Briefly, a sufficiently weak inversion allows the development of evaporatively cooled negatively buoyant downdrafts formed from recently entrained air (but see Albrecht et al., 1985). The downdrafts increase the intensity of the cloud-layer turbulence, and so lead to more rapid entrainment (but see Hanson, 1984). The entrainment process thus becomes selfpromoting (Fig. 3). The resulting rapid entrainment of dry air reduces the humidity of the cloud layer and so leads to a reduction in the fractional cloudiness (but see Randall, 1984).

It is useful to distinguish three phases in the destruction of the uniform cloud layer. In Phase 1, the uniform cloud layer becomes unstable and begins to entrain rapidly; this *initiation* process has been analyzed in the studies cited above. In Phase 2, a *transition* occurs as the uniform cloud layer breaks up into scattered cumuli. This phase is difficult to analyze because, by definition, the cloud layer is not in equilibrium. In Phase 3, *equilibration* occurs as the shallow cumulus regime becomes well established. Phase 3 can be analyzed by using the results derived in section 2.

The turbulent fluxes of moist static energy and total water at the base of an inversion across which the fluxes go to zero and the radiative flux divergence is large satisfy

$$(F_h)_B = -E\Delta h + \Delta R, \tag{4.1}$$

$$(F_r)_B = -E\Delta r, \tag{4.2}$$

where E is the entrainment mass flux, R is the radiative flux, and $\Delta(\ )$ denotes an upward change across the inversion. For the fully overcast case (Phase 1), (4.1–2) and (1.3) imply that

$$(F_{sv})_B = -Ec_p\Delta\sigma_m + \beta\Delta R, \tag{4.3}$$

where $\Delta\sigma_m$ is the "moist" stability parameter defined by Randall (1984), and $\beta(\simeq 0.5)$ is the conventional

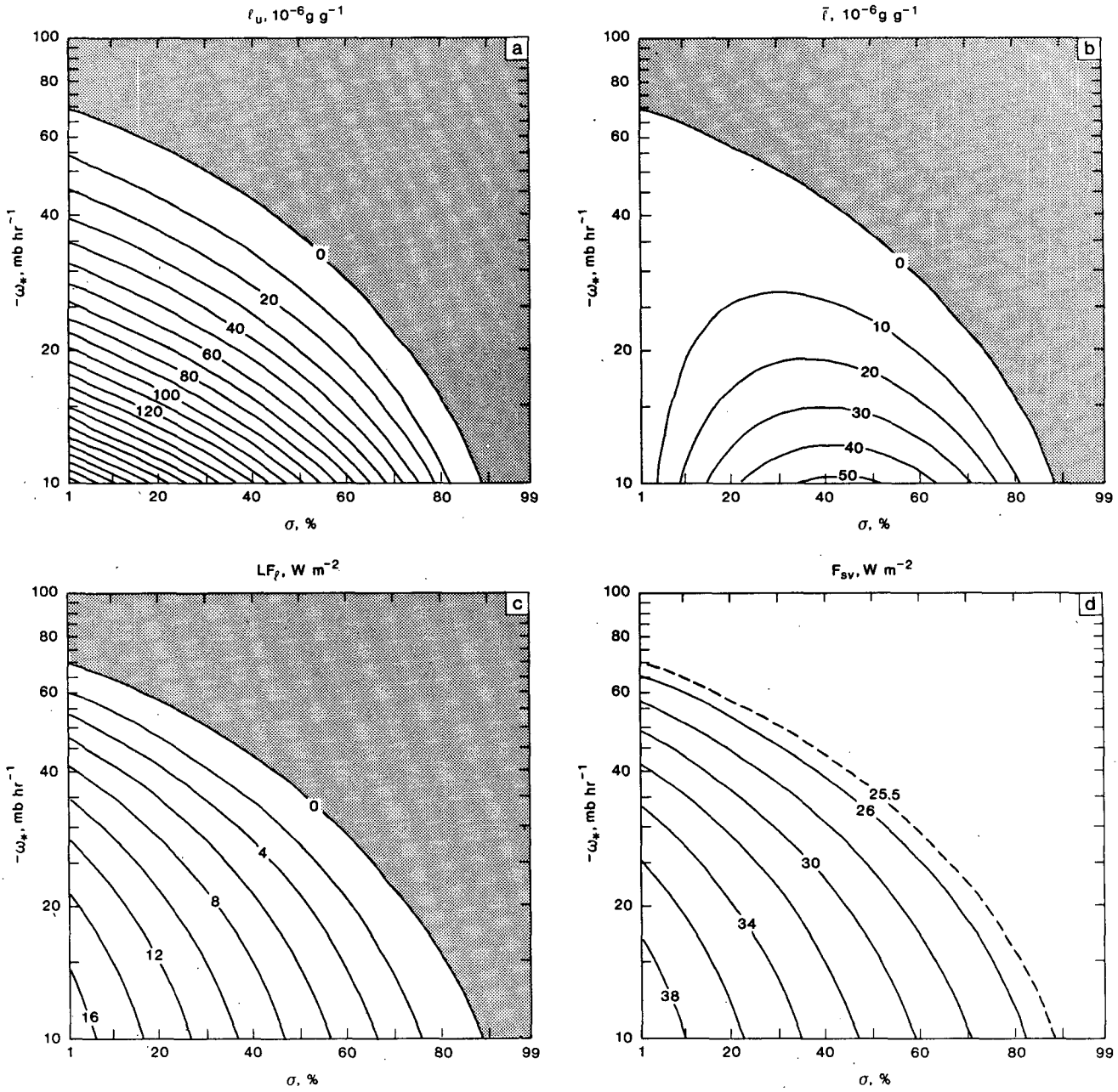

FIG. 1. (a) Variation of l_u with σ and ω_*, for the conditions given in Table 1, contour interval: 0.02 g kg^{-1}. (b) As in (a) but of $\bar{l}$ with σ and ω_*, contour interval: 0.02 g kg^{-1}. (c) As in (a) but of LF_l with σ and ω_*, contour interval: 2 W m^{-2}. (d) As in (a) but of F_{sv} with σ and ω_*, contour interval: 2 W m^{-2}. The dashed line is the 25.5 W m^{-2} contour, where $F_{sv} = (F_{sv})_{CLR}$.

notation for the coefficient of F_h in (1.5). On the basis of (4.3), Randall (1980a) suggested that cloud-top entrainment instability occurs for a uniform cloud layer when $\Delta\sigma_m < 0$, because an increase in E is then accompanied by an increase in $(F_{sv})_B$.

A similar analysis can now be given for Phase 3, in which the updrafts are cloudy and the downdrafts are clear. From (1.2), (1.5), (2.18) and (4.1–2), the buoyancy flux at the inversion base satisfies

$$(F_{sv})_B = -Ec_p[(1-\sigma)\Delta\sigma_m + \sigma\Delta\sigma_d] + \Delta R[(1-\sigma)\beta + \sigma] - \frac{\omega_*}{g}[1-(1+\delta)\epsilon]L\tilde{l}, \quad (4.4)$$

where $\Delta\sigma_d$ is the virtual temperature jump. To avoid unnecessary complications, suppose that the mean state is near saturation, so that $\tilde{l} \approx 0$. To proceed, it is necessary to specify the dependence of ΔR on σ. Radiative

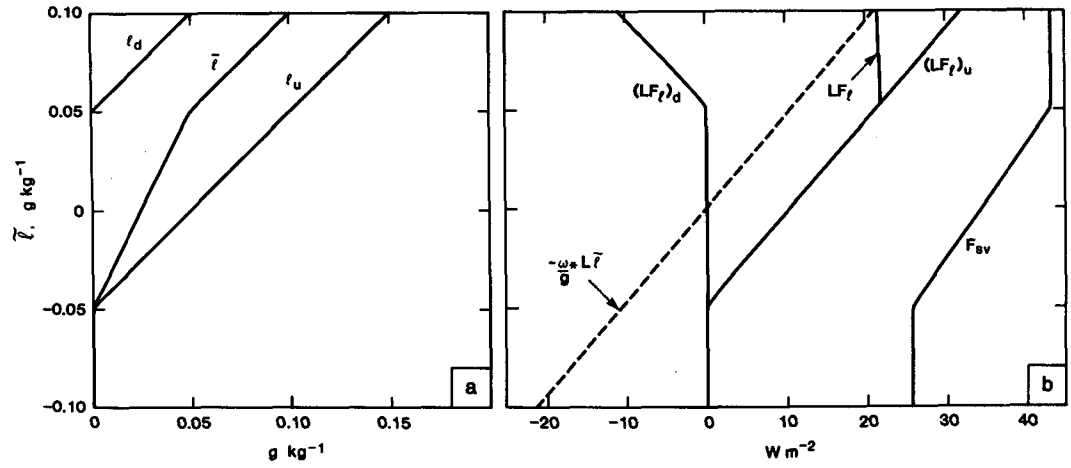

FIG. 2. (a) Variation of l_u, l_d, and $\bar{l}$ with $\tilde{l}$. (b) Variation of $(LF_l)_u$, $(LF_l)_d$, LF_l, $-(\omega_*/g)L\tilde{l}$ and F_{sv} with $\tilde{l}$.

transfer in a partly cloudy layer is a complex and subtle process that is not well understood. For simplicity, we assume that

$$\Delta R = \sigma \Delta R_0, \tag{4.5}$$

where ΔR_0 is the value that ΔR would take in the case of optically thick overcast, with the same upper-level sounding. These assumptions allow us to rewrite (4.4) as

$$(F_{sv})_B = -c_p E[(1-\sigma)\Delta\sigma_m + \sigma\Delta\sigma_d] + \Delta R_0[\sigma^2(1-\beta) + \sigma\beta]. \tag{4.6}$$

This is the "partly cloudy" analogue of (4.3).

According to (4.6), the effects of radiative cooling on the inversion-base buoyancy flux vary quadratically with σ, for given values of E, $\Delta\sigma_m$, $\Delta\sigma_d$, ΔR_0 and β. For small σ, radiative cooling is unimportant, and $(F_{sv})_B \approx -E\Delta\sigma_m$; for σ near one, $(F_{sv})_B \approx -E\Delta\sigma_d + \Delta R_0$. Since both σ and E depend on the turbulence dynamics, however, it is not necessarily useful to consider what happens as they vary "independently". Figure 4 shows the variation of $(F_{sv})_B$ with both σ and E, as given by (4.6), for $\Delta\sigma_d = 5$ K, $\Delta R_0 = 70$ W m^{-2}, $\beta = 0.5$, and for $\Delta\sigma_m = 1$ K (Fig. 4a) and -1 K (Fig. 4b). The sign of $\Delta\sigma_m$ qualitatively influences the results. For $\Delta\sigma_m > 0$ (Fig. 4a), positive values of $(F_{sv})_B$ occur only for large σ and weak entrainment, i.e., for cases in which the radiative cooling term of (4.6) is strong enough to dominate the entrainment term. For all values of σ, $(F_{sv})_B$ decreases as the entrainment rate increases. In contrast, for $\Delta\sigma_m < 0$ (Fig. 4b), $(F_{sv})_B > 0$ occurs for small σ, regardless of the entrainment rate. For sufficiently small σ, $(F_{sv})_B$ actually increases as the entrainment rate increases.

These results suggest that the broken cloud layer of Phase 3 finds it energetically favorable to have small σ and, therefore, small fractional cloudiness. The rapidly entraining, vigorous turbulence developed during Phase 2 will be energetically penalized unless it organizes itself so that σ is small. This argument is similar to that suggested by Asai and Kasahara (1967) to explain the small fractional cloudiness associated with cumulus convection. It is useful to divide Fig. 4b into quadrants, as indicated schematically in Fig. 4c. We expect $(F_{sv})_B > 0$ to promote rapid entrainment, and $(F_{sv})_B < 0$ to inhibit entrainment. From this point of view, only the upper left quadrant is internally consistent.

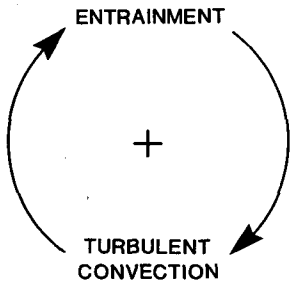

FIG. 3. Positive feedback loop for cloud-top entrainment instability, as analyzed by Randall (1980).

5. Summary and conclusions

A convective mass flux model has been used to derive expressions for the liquid water and buoyancy fluxes. For the case of overcast, the classical results of Lilly (1968) are recovered. For cloudy updrafts and clear downdrafts, the liquid water and buoyancy fluxes increase as the fractional cloudiness decreases, for given fluxes of moist static energy and total water. These results have been interpreted as a consequence of the asymmetry between moist updrafts and clear downdrafts. Examples have been given to illustrate the vari-

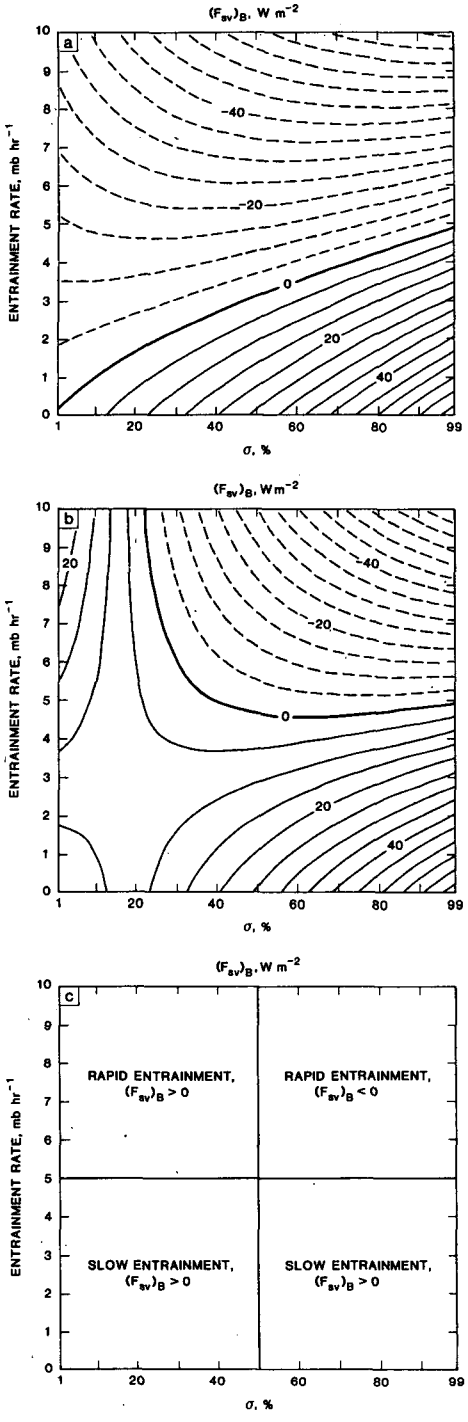

FIG. 4. (a) Variation of $(F_{sv})_B$ with σ and E, as given by (4.6), with $\Delta\sigma_d = 5$ K, $\Delta R_0 = 70$ W m^{-2}, $\beta = 0.5$, and $\Delta\sigma_m = 1$ K. (b) As in (a) but with $\Delta\sigma_m = -1$ K. (c) Schematic idealization of (b).

ations of the fluxes with σ and with the relative humidity of the mean state.

The model has been used to analyze the equilibrated partly cloudy boundary layer that is hypothesized to occur in the aftermath of cloud-top entrainment instability. The results suggest that small fractional cloudiness will occur in this regime.

The ideas presented in this paper help to bridge the gap between cumulus convection as studied by Asai and Kasahara (1967), and stratocumulus convection as studied by Lilly (1968). Such conceptual bridge-building is a prerequisite for understanding the transitions between these two important convective cloud types. In order to carry the present investigation much further, however, it will be necessary to find a way to determine σ and ω_*.

Acknowledgments. A portion of this research was performed while the author was visiting the European Centre for Medium Range Weather Forecasts. Richard Penc of Research and Data Systems Inc. assisted in the use of the STRATEX data. The comments of Drs. Gilles Sommeria, Alan Betts, Chin-Hoh Moeng, Bruce Albrecht, and Howard Hanson are appreciated. Mary Ann Wells and Donna Candido patiently typed the manuscript, and Laura Rumburg drafted the figures. Support has been provided by NASA's Climate Program.

APPENDIX

Applicability of the Model to the STRATEX Data

The results of section 2 are based on a convective mass flux model that is open to question. This Appendix gives a brief discussion of previously published evidence for the model's validity.

Beniston and Sommeria (1981; see also Sommeria, 1976) examined the fluxes and updraft–downdraft anomalies of moist static energy and total moisture produced in a large-eddy simulation of shallow cumulus convection. They showed that a single convective mass flux profile was consistent with both flux profiles. Their Figs. 12 and 13 indicate that the liquid water flux is qualitatively consistent with the same mass flux. The present study shows that it is particularly important for the mass flux model must past this additional test.

Albrecht et al. (1985) and Penc and Albrecht (1986; hereafter PA) presented an analysis of the boundary-layer cloud observations collected by the NCAR Electra during STRATEX, which was conducted off the coast of California in June 1976. On 13 June (Flight 4), the aircraft flew through broken clouds that filled most of the marine layer. From filtered turbulence data collected on this flight, Penc and Albrecht determined the turbulent fluxes of potential temperature, water vapor, and liquid water at 6 levels. They used the same filtered data to determine updraft and downdraft properties. Soundings of the mean temperature, water vapor mixing ratio, and liquid water mixing ratio were also recorded. The data are summarized in Table 2.

Penc and Albrecht partitioned their data into three domains: updrafts, downdrafts, and an environment. The particular method used will be discussed later. As-

TABLE 2. STRATEX data for 13 June 1976, as analyzed by Albrecht et al. (1985) and Penc and Albrecht (1986).

z, m	p (mb)	$\bar{h}/c_p$ (K)	$\bar{r}$ (g kg^{-1})	$\bar{l}$ (g kg^{-1})	RH (%)	$\tilde{l}$ (g kg^{-1})	F_h (W m^{-2})	LF_r (W m^{-2})	LF_l (W m^{-2})	σ_u	σ_d	ω_* (mb h^{-1})
600	949.0	311.7	8.190	0.000	87.2	−0.466	1.0	1.7	0.0	0.26	0.27	−10.0
490	962.9	309.5	8.315	0.035	97.7	−0.044	4.1	11.4	5.0	0.26	0.31	−17.4
365	977.3	308.9	8.448	0.078	97.5	−0.011	18.5	22.4	5.0	0.27	0.30	−31.5
275	987.9	308.9	8.559	0.049	97.0	−0.057	23.4	30.5	6.4	0.30	0.32	−36.4
180	998.9	309.0	8.708	0.018	96.4	−0.113	31.1	36.2	3.5	0.30	0.34	−36.6
60	1013.8	309.1	8.850	0.000	93.9	−0.224	32.8	23.0	0.0	0.28	0.34	−41.0

sume for simplicity that the environment has the same properties as the mean state. The mass flux model presented in section 2 needs only minor revision to deal with this more general case. In particular, (2.1) and (2.4) must be replaced by

$$\bar{\Psi} = \sigma_u \Psi_u + \sigma_d \Psi_d + [1 - (\sigma_u + \sigma_d)]\bar{\Psi}, \tag{A1}$$

$$\omega_* = \left(\frac{\sigma_u \sigma_d}{\sigma_u + \sigma_d}\right)(\omega_u - \omega_d), \tag{A2}$$

respectively; no change is needed in (2.3). The results (2.17) and (2.18) still apply if $1 - \sigma$ is replaced by $\sigma_d/(\sigma_u + \sigma_d)$. If the mean vertical motion is negligible, *both* (2.4) and (A2) reduce to

$$\omega_* \approx \sigma_u \omega_u. \tag{A3}$$

Penc and Albrecht used (A3) to determine the values of ω_* given in Table 2 (their Fig. 9c). They also evaluated ω_* using

$$\omega_* = -gF_l/(l_u - l_d), \tag{A4}$$

where l_u and l_d were determined by conditional sampling (their Fig. 4); corresponding ω_* profiles were obtained from potential temperature and equivalent potential temperature data. They found "good" agreement between their four independently determined profiles of ω_* (their Fig. 9a) and interpreted this agreement as evidence that the convective mass flux model can be used to represent the liquid water fluxes in partly cloudy layers.

Just how "good" are the results of PA's observational test of the mass flux model? One way to answer this question is to check the mutual consistency of the updraft and downdraft thermodynamic properties implied by the model, for a particular convective mass flux profile. The observed values of ω_* and F_l given in Table 2 can be used to evaluate $l_u - l_d$ from (A4), and a similar method can be used to determine $h_u - h_d$ and $r_u - r_d$. Then (A1) can be combined with the observed values of σ_u, σ_d, $\bar{l}$, $\bar{h}$ and $\bar{r}$ to determine l_u, l_d, h_d, h_u, h_d, r_u and r_d. The results are given in Table 3. Notice that l_u and l_d are both positive between 180 and 490 m; the updrafts and downdrafts both contain liquid. This indicates that the clear air encountered by the aircraft was in the "environment" between the updrafts and the downdrafts. Certainly the mean state was subsaturated, as shown by the profiles of relative humidity and $\tilde{l}$ given in Table 2.

A very tough test of the model (and the data) can now be performed. The values of h_u and r_u given in Table 3 can be used to check for saturation and the presence of liquid water in the updrafts. This gives an independent estimate of l_u, which we call $(l_u)_x$ to distinguish it from the value of l_u given in Table 3. In a similar way we can obtain an independent estimate of l_d, which we call $(l_d)_x$. There is no guarantee that $l_u = (l_u)_x$ or $l_d = (l_d)_x$. When no liquid is found in the updraft, we put $(l_u)_x = r_u - q_u^* < 0$, and similarly for the downdraft. The values of $(l_u)_x$ and $(l_d)_x$ (and their difference) are given in Table 4; the agreement with l_u and l_d (and their difference) is not very encouraging.

Unfortunately, it is all too easy to make excuses for this apparent failure of the model, by appealing to the weaknesses of the observations and the methods used to analyze them. Among the difficulties are these:

1) PA grouped the data into "updrafts" and "downdrafts" by using criteria that involve both vertical velocity and humidity, rather than vertical velocity

TABLE 3. Updraft and downdraft properties consistent with the data of Table 2.

z, m	l_u (g kg^{-1})	l_d (g kg^{-1})	$l_u - l_d$ (g kg^{-1})	h_u/c_p (K)	h_d/c_p (K)	r_u (g kg^{-1})	r_d (g kg^{-1})
600	0.000	0.000	0.000	311.7	311.7	8.202	8.178
490	0.057	0.017	0.040	309.6	309.5	9.365	8.273
365	0.089	0.067	0.022	309.0	308.8	8.500	8.400
275	0.061	0.037	0.024	309.0	308.8	8.619	8.501
180	0.025	0.012	0.013	309.2	308.9	8.782	8.643
60	0.000	0.000	0.0000	309.3	309.0	8.893	8.814

TABLE 4. Updraft and downdraft profiles of $r - q^*$, determined from the values of h_u, h_d, r_u, and r_d given in Table 3.

z, m	$(l_u)_x$ (g kg^{-1})	$(l_d)_x$ (g kg^{-1})	$(l_u)_x - (l_d)_x$ (g kg^{-1})
600	−1.177	−1.217	
490	−0.010	−0.187	0.077
365	0.016	−0.086	0.102
275	−0.060	−0.217	0.157
180	−0.194	−0.361	0.167
60	−0.560	−0.587	

alone. In contrast, the model distinguishes updrafts from downdrafts purely on the basis of vertical velocity.

2) Liquid water content was sampled only once per second, and only over a portion of the droplet spectrum. Large sampling errors are therefore expected. Turbulence statistics such as l_u, l_d and F_l are particularly vulnerable to such errors.

3) As discussed by Penc and Albrecht the data were filtered before statistics were computed, in order to remove the effects of the mesoscale. The filtered fluxes of all variables are quite different from the corresponding unfiltered values. The filter may have affected the mean liquid water content, since the local liquid water content is a positive definite quantity. It is not clear how the filtering has affected the analysis given above.

4) Our analysis is very sensitive to small systematic biases in the measurements of the mean temperature and/or vapor mixing ratio, simply because the liquid water mixing ratios that we are dealing with are much smaller than either the actual vapor or saturation vapor mixing ratios.

The first problem can be avoided by revising the conditional sampling strategy used to analyze the observations. The remaining three problems are difficult to solve with real data and present technology, but would not occur with model "data" generated in a large-eddy simulation of the type reported by Deardoff (1980a,b), Moeng (1984) and Moeng and Wyngaard (1985).

REFERENCES

Albrecht, B. A., R. S. Penc and W. H. Schubert, 1985: An observational study of cloud-topped mixed layers. *J. Atmos. Sci.*, **42**, 800–822.

Arakawa, A., 1969: Parameterization of cumulus convection. *Proc. WMO/IUGG Symp. Numerical Weather Prediction*, Tokyo, 26 November–4 December, 1968, Japan Meteor. Agency, IV, **8**, 1–6.

Asai, T., and A. Kasahara, 1967: A theoretical study of the compensating downward motions associated with cumulus clouds. *J. Atmos. Sci.*, **24**, 487–496.

Banta, R., and W. R. Cotton, 1980: On computing average cloud-water quantities in a partially cloudy region. *J. Rech. Atmos.*, **14**, 487–492.

Beniston, M. G., and G. Sommeria, 1981: Use of a detailed planetary boundary layer model for parameterization purposes. *J. Atmos. Sci.*, **38**, 780–797.

Betts, A. K., 1973: Non-precipitating cumulus convection and its parameterization. *Quart. J. Roy. Meteor. Soc.*, **99**, 178–196.

Bjerknes, J., 1938: Saturated-adiabatic ascent of air through dry-adiabatically descending environment. *Quart. J. Roy. Meteor. Soc.*, **64**, 325–330.

Bougeault, Ph., 1981: Modeling the trade-wind cumulus boundary layer. Part I: Testing the ensemble cloud relations against numerical data. *J. Atmos. Sci.*, **38**, 2414–2428.

——, 1982: Cloud-ensemble relations based on the gamma probability distribution for the higher-order models of the planetary boundary layer. *J. Atmos. Sci.*, **39**, 2691–2700.

Deardoff, J. W., 1980a: Cloud top entrainment instability. *J. Atmos. Sci.*, **37**, 131–147.

——, 1980b: Stratocumulus-capped mixed layers derived from a three-dimensional model. *Bound. Layer Meteor.*, **18**, 495–527.

Hanson, H. P., 1984: Stratocumulus instability reconsidered: A search for physical mechanisms. *Tellus*, **36A**, 355–368.

Lilly, D. K., 1968: Models of cloud-topped mixed layers under a strong inversion. *Quart. J. Roy. Meteor. Soc.*, **94**, 292–309.

Mellor, G. L., 1977: The Gaussian cloud model relations. *J. Atmos. Sci.*, **34**, 356–358.

Moeng, C.-H., 1984: A large-eddy simulation model for the study of planetary boundary-layer turbulence. *J. Atmos. Sci.*, **41**, 2052–2062.

——, and J. C. Wyngaard, 1985: The structure of a stratus-topped PBL as seen through large-eddy simulation. *Report of the JSC/CAS Workshop on Modeling of Cloud-Topped Boundary Layer, WMO* (Appendix I).

Oliver, D. A., W. S. Lewellen and G. G. Williamson, 1978: The interaction between turbulent and radiative transport in the development of fog and low-level stratus. *J. Atmos. Sci.*, **35**, 301–316.

Randall, D. A., 1976: The interaction of the planetary boundary layer with large-scale circulations. Ph.D. thesis, The University of California, Los Angeles, 247 pp.

——, 1980a: Conditional instability of the first kind, upside-down. *J. Atmos. Sci.*, **37**, 125–130.

——, 1980b: Entrainment into a stratocumulus layer with distributed radioactive cooling. *J. Atmos. Sci.*, **37**, 148–157.

——, 1985: Key problems of parameterization for cloud-topped boundary layers. *Proc. Workshop on the Modelling of the Cloud-Topped Boundary Lay.*, World Climate Research Program, Fort Collins, Appendix J.

Sommeria, G., 1976: Three-dimensional simulation of turbulent processes in an undisturbed trade-wind boundary layer. *J. Atmos. Sci.*, **33**, 216–241.